Effects of Fluorination on Self-Assembled Monolayer Formation from Alkanephosphonic Acids on Aluminum: Kinetics and Structure

Mark J. Pellerite,*,‡ Timothy D. Dunbar,† Larry D. Boardman,† and Erika J. Wood‡

Interface Materials Technology Center and Organic Materials Technology Center, 3M Company, 3M Center 201-1W-28, St. Paul, Minnesota 55144

Received: May 22, 2003; In Final Form: August 7, 2003

We have used infrared spectroscopy, ellipsometry, and contact angle measurements to study self-assembled monolayer (SAM) formation on aluminum native oxide from three alkanephosphonic acids: $CF_3(CF_2)_7(CH_2)_{11}PO_3H_2$ ($F_8H_{11}PA$), and $CH_3(CH_2)_nPO_3H_2$ ($n = 15$ ($H_{16}PA$); $n = 21$ ($H_{22}PA$)). These compounds show significant differences in film structure and film formation kinetics. Strikingly, the methylene segment of the semifluorinated $F_8H_{11}PA$ SAM never reaches an ordered state even at long assembly times. This contrasts with the ordered chains in equilibrium films from $H_{16}PA$ and $H_{22}PA$. We attribute this behavior to steric effects of the fluorocarbon segment and the phosphonic acid headgroup. $F_8H_{11}PA$ represents an amphiphile in which bulky head and tail groups prevent an interposed hydrocarbon segment from ordering. For all three phosphonic acids, negative peaks attributed to loss of Al−OH groups in the infrared spectra of the monolayers are consistent with a condensation reaction between the acids and surface hydroxyls to form bound aluminophosphonate salts. With respect to kinetics, our results indicate that $F_8H_{11}PA$ approaches its equilibrium film structure considerably faster than the hydrocarbon phosphonic acids. We interpret the structural dependence of film formation kinetics in terms of the T_c formalism advanced by Rondelez and co-workers (*Langmuir* **1994**, *10*, 4367−4373). We also suggest that the accelerated film formation exhibited by $F_8H_{11}PA$ may be due to chain entanglement and solubility effects, to the extent that this species may self-assemble as islands of approximately vertically oriented chains which fill in as coverage increases. $H_{22}PA$ may also deposit as islands, but in contrast, film formation for $H_{16}PA$ probably involves initially disordered chains with higher tilt angles that order and reorient as film assembly proceeds.

Introduction

Self-assembled monolayers (SAMs) of organic amphiphiles on metal and metal oxide substrates have been studied extensively over the past 20 years.[1,2] In addition to its purely scientific importance, this technology is making inroads in applications such as surface passivation and corrosion protection,[2d,f] lubrication,[2d] oil and water repellency,[3] biosensors,[2d,f] electro-optics,[2d] and interfacial control in organic electronic devices.[4] The quintessential SAM systems, alkanethiols on gold and alkylsilanes on silica, have been scrutinized using virtually every tool in the surface science arsenal, and a voluminous literature exists.[2] Another important class of self-assembling materials, phosphonic acids, is somewhat less well characterized, but is becoming of great practical interest because of the ability of these materials to produce robust, well-anchored monolayers on a wide range of metal oxide surfaces.[4e,5−29] Phosphonic acids undergo monolayer formation on many substrates by condensation reactions of the acid function with metal hydroxyl species to form bound phosphonate salts.[9,10,17,18,23,28,29] Much of the phosphonic acid literature to date is devoted to the characterization of hydrocarbon systems, and little information is available on the behavior of fluorinated phosphonic acid SAMs.

Fluorinated monolayers are of current interest on several levels. First, like other fluorinated surfaces, they can display properties such as high contact angles against hydrocarbon liquids, which are not found with their hydrocarbon counterparts.[30] They are also significant from a more fundamental standpoint, with respect to effects of fluorine substitution on film assembly and structure. Although well studied for thiol[31−45] and silane[46,47] amphiphiles, these issues have not yet been widely investigated within the framework of other self-assembling monolayer chemistries.[48]

In this paper, we present results from a study of self-assembled monolayers from partially fluorinated phosphonic acid **1** (referred to below as $F_8H_{11}PA$) on aluminum. This molecule is particularly appropriate for our study since it has well-defined fluorocarbon and hydrocarbon segments that are amenable to investigation by infrared spectroscopy. SAM properties and formation kinetics are elucidated using infrared, ellipsometry, and contact angle measurements, and the results compared to those for *n*-hexadecanephosphonic acid **2** ($H_{16}PA$) and *n*-docosanephosphonic acid **3** ($H_{22}PA$) as well as literature results on other self-assembled monolayer systems with similar alkyl group structures. The hydrocarbon systems studied here bracket the semifluorinated species with respect to chain length. We see striking differences in the behavior of these fluorinated and hydrocarbon molecules under the conditions studied, and we conclude by proposing a mechanistic rationale of our observations.

* Corresponding author. E-mail: mjpellerite1@mmm.com.
† Interface Materials Technology Center, 3M Co.
‡ Organic Materials Technology Center, 3M Co.

$CF_3(CF_2)_7(CH_2)_{11}PO_3H_2$ **1** $CH_3(CH_2)_{15}PO_3H_2$ **2** $CH_3(CH_2)_{21}PO_3H_2$ **3**

10.1021/jp0354200 CCC: $25.00
Published on Web 09/25/2003

Experimental Section

Materials. All solvents and reagents were standard commercial grade and used as received. Experimental details for the preparations of the three phosphonic acids utilized in this study—**1** ($F_8H_{11}PA$), **2** ($H_{16}PA$), and **3** ($H_{22}PA$)—are provided in the Supporting Information. Water (18.2 MΩ) for contact angle measurements was drawn from a Millipore deionized water filtration system. Hexadecane was of commercial anhydrous grade and used as received. Aluminum-coated silicon wafers (100 mm diameter, 500 nm PVD aluminum) were obtained from WaferNet (San Jose, CA). Analysis of the substrate by AFM revealed a rough surface consisting of irregularly shaped grains ranging in size from 0.3 to 1.0 μm.

Film Preparation. Aluminum-coated wafers were cut into quarters and cleaned by 5−10 min exposure in a home-built UV/ozone chamber under a gentle flow of oxygen. This treatment yielded a completely hydrophilic substrate with a water contact angle of essentially zero. Immediately after cleaning, the wafer pieces were immersed in a fresh 0.1 wt % solution of the desired phosphonic acid for times ranging from 5 s to 4 weeks. Films of $F_8H_{11}PA$ and $H_{16}PA$ were deposited from absolute ethanol, films of $H_{22}PA$ from tetrahydrofuran due to its low solubility in ethanol. After coating, the wafer pieces were rinsed in fresh solvent (denatured alcohol was used as the rinse for phosphonic acids **1** and **2**) by vigorous agitation by hand for 1 min in a beaker of the liquid, then blown dry under nitrogen. To verify that the tetrahydrofuran rinse of films of $H_{22}PA$ was effective in removal of any excess unbound amphiphile, several runs were made in which samples were rinsed by sonication for 5 min in tetrahydrofuran. No significant difference was noted between samples rinsed with and without sonication. Finally, as a check that solvent effects are unimportant in these systems, several runs were made with $H_{16}PA$ and $F_8H_{11}PA$ in THF solution instead of ethanol. No significant differences were observed in the results, although sonication was necessary for removal of excess deposits of $F_8H_{11}PA$. Ethanol is our preferred solvent for these compounds because in our hands THF solutions tended to be less stable, and they occasionally developed a precipitate within a few days of preparation.

Film Characterization: Infrared Spectroscopy. Infrared reflection absorption spectroscopy (IR−RAS) was performed using a Biorad FTS-175C spectrometer equipped with a liquid nitrogen-cooled wide band MCT detector. The reflection spectra were collected employing a Graseby-Specac variable angle external reflection accessory, mounted in the sample chamber, set to reflect light at an angle of 82° measured from the surface normal. A wire grid polarizer was mounted on the accessory and was aligned to allow only p-polarized radiation to reflect from the surface. Immediately after cleaning (see above), a sample was placed in the spectrometer and a reference spectrum of 400 scans was collected. The sample was removed, and initial ellipsometry data were collected. The wafer piece was then treated with the desired phosphonic acid as described above, and reinserted into the spectrometer. An additional 400 scans were run, and this sample spectrum was ratioed to the reference spectrum obtained from the uncoated wafer. Another reference sample was prepared by immersing a cleaned aluminum wafer piece in a solution of 0.1% $CD_3(CD_2)_{15}PO_3H_2$ in isopropyl alcohol for at least a day. This sample has essentially no features in the C−H stretching region of its IR−RAS spectrum. It was used to verify that the C−H stretching region of the IR was stable over the 1−4 weeks between collection of reference and sample spectra for our longest dip time samples. Spectra in which water vapor appeared in the low-frequency region were subtracted using a spectrum of water vapor collected on the instrument.

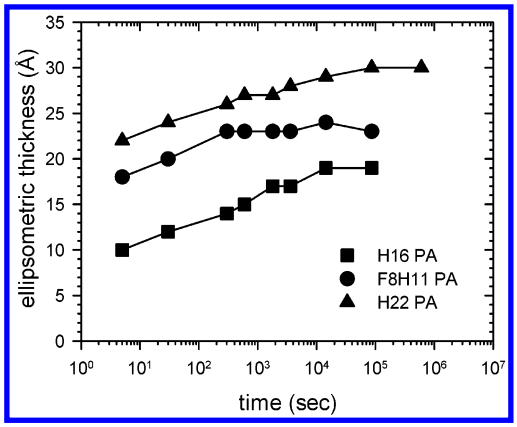

Figure 1. Ellipsometric film thickness vs immersion time for phosphonic acid self-assembled films on aluminum. See text for film formation conditions and details of extraction of thickness from ellipsometric parameters. Experimental uncertainty in the thickness is estimated at ±2 Å.

Film Characterization: Ellipsometry. Using a Gaertner (Skokie, IL) L116A single-wavelength ellipsometer operating at 6328 Å and 70° incident angle, ellipsometric parameters Ψ and Δ were measured on the same four spots before and after coating. Film thicknesses were determined from these values[49] using software supplied with the instrument, a three-layer model (air/film/substrate,) and assumed values for the film refractive index ($n_f = 1.38$ for phosphonic acid **1**, $n_f = 1.45$ for **2** and **3**.) Experimental uncertainty in the thickness is estimated at ±2 Å.

Film Characterization: Contact Angles. Static and dynamic contact angles were measured using an AST Products (Billerica, MA) VCA-2500XE video contact angle (VCA) apparatus. Values reported are averages of measurements on both sides of at least three drops, on at least two samples prepared on different days. Liquid drops of volume 5 μL were used in static measurements, and drops of 1−3 μL, for dynamic measurements. Hexadecane static contact angles are not reported here, since they were always found to be extremely close to the advancing values. Estimated uncertainties in the contact angles were ±1° for static and advancing angle measurements, and ±2° for receding angle measurements.

Results and Discussion

Ellipsometry and Contact Angles for Phosphonic Acid SAMs. Film formation from $F_8H_{11}PA$ on aluminum-coated silicon wafers was monitored by ellipsometry and contact angle measurements as a function of immersion time in 0.1 wt % solutions (1.2 mM) of the phosphonic acid in absolute ethanol. Immersion times ranged from 5 s to 24 h, and results from these studies appear in Figure 1 and Table 1.

$F_8H_{11}PA$ showed rapid film growth on aluminum, with ellipsometric film thickness, water static and advancing contact angles, and hexadecane contact angles all reaching their equilibrium (24 h) values within 5−10 min. A small increase in receding angles is evident out to 24 h immersion time, perhaps indicating additional chain orientation occurring on this time scale. We address this behavior in greater detail in the discussion of infrared spectra (see below).

Significant film formation and autophobicity was even noted at dip times as short as 5 s. It has been suggested in the literature[20,24] that this may be due to Langmuir-type film transfer

TABLE 1: Contact Angles vs Immersion Time for $F_8H_{11}PA$ Self-assembled Films on Aluminum

dip time	$F_8H_{11}PA$ water static/adv/rec CA (deg)	$F_8H_{11}PA$ hexadecane adv/rec CA (deg)
5 s	117/123/104	74/67
30 s	120/124/113	77/68
5 min	122/125/116	78/67
10 min	121/125/113	77/70
30 min	121/125/117	77/70
1 h	122/125/117	79/70
4 h	122/125/117	79/70
24 h	122/125/119	78/70

TABLE 2: Water Contact Angles vs Immersion Time for Hydrocarbon Phosphonic Acid Self-Assembled Films on Aluminum

dip time	$H_{16}PA$ water static/adv/rec CA (deg)	$H_{22}PA$ water static/adv/rec CA (deg)
5 s	101/107/82	109/115/94
30 s	104/108/86	110/115/98
5 min	107/111/96	112/116/101
10 min	109/112/96	110/116/99
30 min	109/113/97	111/116/99
1 h	110/114/99	112/115/101
4 h	111/114/99	111/116/99
24 h	108/114/96	109/116/101
7 days	- - -	111/116/101

as the substrate is withdrawn through the solution/air interface, assuming the presence of a surface excess of the amphiphile. We do not believe this occurs in this system, based on the following experimental data. First, the static surface tension[50] of 0.1 wt % **1** in absolute ethanol was not significantly different from that of pure ethanol, indicating little or no surface activity in this solvent. Second, for comparison, the immersion coating was also done using a modified procedure. In this method, the wafer was never inserted or withdrawn through the 0.1 wt % solution/air interface, thus eliminating any possibility for Langmuir-type film transfer. This was accomplished by starting with the wafer under pure solvent in a small Petri dish, and then quickly adding an aliquot of a stock solution of phosphonic acid so as to bring the concentration to 0.1 wt %. The wafer was left for the desired immersion time (5 or 30 s), then film formation was quenched by submerging the Petri dish in a large reservoir (1 L) of pure solvent to dilute the phosphonic acid by a factor of about 100. The Petri dish was withdrawn, still filled with liquid, then immersed in a second 1 L reservoir of pure solvent before the wafer was finally withdrawn and blown dry. This procedure gave film thickness essentially identical to those obtained by simply immersing in and withdrawing from the 0.1 wt % phosphonic acid solution, indicating that the significant film thicknesses built up after short immersion times are actually due to film growth and not Langmuir-type film transfer.

Water contact angles for $F_8H_{11}PA$ monolayers on aluminum (adv/rec = 125°/119°, Table 1) compare favorably with the values (adv/rec = 122°/117°) reported by Fukushima and co-workers[37] for the partially fluorinated thiol $C_{10}F_{21}(CH_2)_{11}SH$ ($F_{10}H_{11}$ thiol) on gold. Hexadecane values for the phosphonic acid (adv/rec = 79°/70°) are slightly lower than those reported for the $F_{10}H_{11}$ thiol (adv/rec = 83°/75°), perhaps due to a substrate effect or the shorter fluorocarbon segment. A greater sensitivity of alkane contact angles than those of water to fluorocarbon group structure has also been noted in monolayers prepared from fluorinated trichlorosilanes.[47]

Film growth kinetics, as measured by ellipsometry, for the hydrocarbon phosphonic acids (Figure 1) displayed quite different behavior from that for $F_8H_{11}PA$. Whereas the latter had leveled out at its equilibrium value by 10 min immersion in 1.2 mM solution, both H_{16} and H_{22} required at least 4 h to achieve their equilibrium film thickness, even at amphiphile molar concentrations (0.1 wt % $H_{16}PA$ in absolute ethanol is 2.6 mM, 0.1 wt % $H_{22}PA$ in THF is 2.3 mM) roughly double that used for $F_8H_{11}PA$. If monolayer formation were diffusion-controlled, self-assembly would be expected to be faster for the lighter hydrocarbon phosphonic acids. That the opposite is observed suggests fundamentally different mechanisms at work governing film formation for the two types of phosphonic acids.

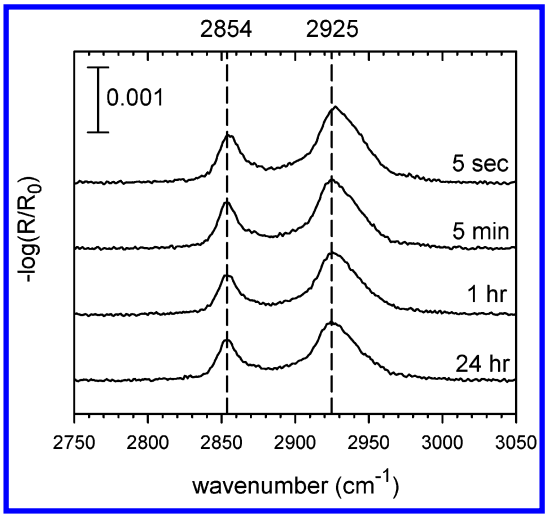

Figure 2. IR−RAS spectra of the C−H stretching region of $F_8H_{11}PA$ SAMs on aluminum as a function of immersion time.

Water contact angles for $H_{16}PA$ and $H_{22}PA$ were significantly lower (Table 2) than those for the fluorinated species. This is in accord with literature data, as an increase in water contact angles upon fluorine substitution is commonly observed in self-assembled monolayer systems.[44,45,51] The contact angle vs time behavior for the two hydrocarbon phosphonic acids is also quite different. Whereas $H_{16}PA$ gave static and advancing angles that steadily increased out to about 1 h immersion time, $H_{22}PA$ behaved more like the fluorocarbon system in that little change in contact angles occurred after 5 min immersion. This difference is a manifestation of the differences in alkyl chain length and the effects this parameter has on film growth and chain ordering as a function of immersion time. Thus, these data, taken together with the infrared data discussed below, suggest that the observed contact angles are a sensitive function of surface coverage and chain ordering.

Infrared Spectral Behavior of Phosphonic Acid SAMs. $F_8H_{11}PA$. IR−RAS kinetic data on self-assembled films of $F_8H_{11}PA$ on aluminum are summarized in Figures 2 and 3. The vibrational modes of the $F_8H_{11}PA$ monolayers are listed in Table 3. Assignments were made largely based upon data in refs 38, 42, 43, and 52 and references therein.

The bands attributed to the fluorocarbon and hydrocarbon portions of the molecule display quite different time-dependent behavior. In the C−H stretching region of the spectra, only minor changes occurred as a function of immersion time in the coating solution (Figure 2). Figure 4 shows that the methylene portion of the F_8H_{11} chain does not become significantly more ordered after 5 s immersion. The peak positions after 5 s were 2855 and 2927 cm^{-1} for the methylene symmetric d^+ and asymmetric d^- modes, respectively, whereas in the 24 h dip sample, they decreased only to 2854 and 2925 cm^{-1}. Such peak shifts indicate only a modest amount of conformational ordering, differing from the more ordered state of a polycrystalline

TABLE 3: Infrared Vibrational Modes for $F_8H_{11}PA$, in Bulk and in Self-assembled Films on Aluminum

		mode frequency (cm^{-1}) and relative intensity				
			monolayer immersion times			
mode description	transition dipole moment direction[a]	bulk	5 s	5 min	1 h	24 h
$\nu_a(CH_2)$, d^-	⊥, ⊥ to CCC plane	2920 m	2927 w	2925 w	2926 w	2925 w
$\nu_s(CH_2)$, d^+	⊥, in CCC plane	2851 m	2855 w	2854 w	2854 w	2854 w
(CH_2) scissors	⊥	1471 m	1470 vw	1470 vw	1467 vw	1468 vw
$\nu(CF_2)$ progression, axial CF_2 stretch	||	1372 w	1373 w	1373 m	1373 s	1373 s
$\nu(CF_2)$ progression, axial CF_2 stretch	||	1334 w	1333 m	1334 s	1335 vs	1335 vs
$\nu_a(CF_2)$ and $r(CF_2)$	⊥	1250 sh, 1233 sh	1252 vs	1248 m	1247 m	1247 m
$\nu_a(CF_2) + \nu_a(CF_3)$	⊥	1212 sh	1216 m	1218 sh	1217 sh, 1221 sh	1217 sh, 1222 sh
$\nu_a(CF_2) + \nu_a(CF_3)$	⊥	1201 vs	1205 sh	1206 w	1206 w	1205 w
$\nu_s(CF_2)$, $\delta(CF_2)$	⊥	1146 vs	1155 s	1152 s	1152 m	1151 m
unassigned		1135 sh	1137 vw	1138 vw	1138 w	1138 vw
$\nu(CC)$		1114 m	1118 w	1119 m	1119 m	1119 m
$\nu(CC)$		1077 m				
$\nu_s(PO_3^{2-})/\nu(PO_2H^-)$			1055 br	1072 br	1074 br	1075 br
$\nu_a(P-O)$		1002 s				
CF_3		980 sh		977 vw	977 vw	977 w
unassigned		949 sh	953 vw	953 vw	954 w	954 w
$\nu_s(P-O)$		938 w				
CF_2 prog (ν_3)		880 vw	872 vw	873 vw	872 vw	873 vw
(CF_3) symm. def		748 vw	749 vw	749 vw	749 vw	749 vw
$r(CH_2)$	⊥	722 w	722 w	723 w	723 w	723 w
$r(CF_2)$, $wag(CF_2)$	||	706 m	705 w	706 s	706 s	706 vs
$wag(CF_2)$	||	668 m	658 m	662 vs	663 vs	663 vs

[a] Transition dipole moment direction with respect to chain axis (methylene chain) or chain helix (fluorocarbon chain): ||, parallel; ⊥, perpendicular; δ, bend; FR, Fermi resonance; ip, in plane; ip CCC, in plane of the all-trans carbon backbone; r, rock; sh, shoulder; s, strong; m, medium; w, weak; ν_a, asymmetric stretch; ν_s, symmetric stretch.

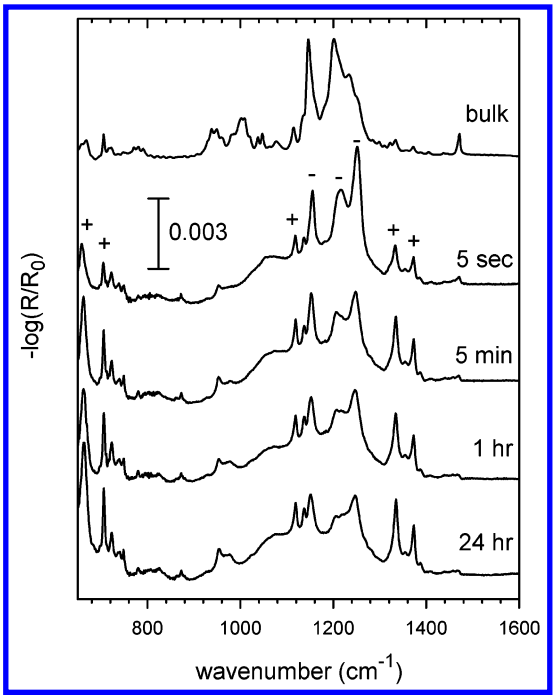

Figure 3. IR−RAS spectra of the fingerprint region of $F_8H_{11}PA$ SAMs on aluminum as a function of immersion time. IR−RAS spectra are labeled by their immersion time in solution. Peaks marked with "+" increase in intensity as a function of time in solution, while those marked with "−" decrease in intensity. Also included is a spectrum (top spectrum, scaled to match the reflection spectra) of the bulk compound dispersed in KBr.

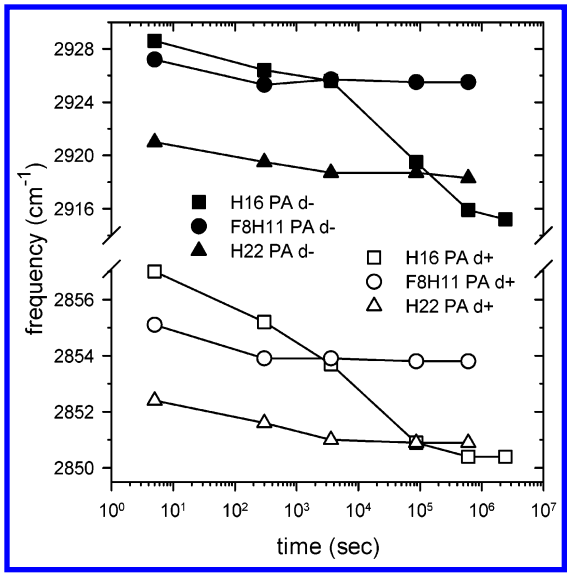

Figure 4. Plots of peak frequency vs immersion time for $H_{16}PA$ (squares), $F_8H_{11}PA$ (circles), and $H_{22}PA$ (triangles) assemblies on aluminum. Filled symbols are for the d^- mode (CH_2 asymmetric stretch) and open symbols are for the d^+ mode (CH_2 symmetric stretch).

$F_8H_{11}PA$ sample dispersed in KBr, where the d^+ and d^- peak positions are 2852 and 2920 cm^{-1}, respectively. This lack of ordering of the methylene segments of the $F_8H_{11}PA$ molecule as it self-assembles is in stark contrast to literature data reported on semifluorinated alkanethiols. $F_{10}H_{11}$ thiol self-assembled for 24 h on either gold[37] or silver[38] substrates gave d^+ and d^- modes observed at 2850−2851 and 2919 cm^{-1}, respectively. A similar study on F_8H_{11} thiol reported these frequencies at 2850 and 2918 cm^{-1} for this compound on gold.[42] This difference between the two chemistries may be related to the fact that the phosphonic acid headgroup is larger than the thiol headgroup, or perhaps to a lower mobility of phosphonates on the aluminum surface relative to thiols on silver or gold surfaces.

Though there were only slight changes with immersion time in the intensity of the two methylene bands, they hide a larger change in orientation. The 5 s sample had an ellipsometric thickness of 18 Å, while that after 24 h was 23 Å (Figure 1.)

The fact that greater coverage lead to an even smaller signal indicates that the methylene chains orient more toward the surface normal with increasing coverage/immersion time.

We note here an interesting feature observed in the high-frequency region of all phosphonic acid SAM spectra on aluminum. Regardless of the time in solution, two weak negative peaks appeared, one at about 3700 cm^{-1}, the other near 3740 cm^{-1}. These O−H[53] stretches arise due to the removal of hydroxyl groups from the oxidized aluminum surface due to reaction with the phosphonic acid monolayer and formation of the corresponding aluminophosphonate salt. The disappearance of hydroxyl groups from the surface is noteworthy as an indication of the condensation reaction that occurs between the phosphonic acid (P−OH) and the alumina-like surface (Al−OH). (A clean Al-coated wafer was used as the reference in these experiments, with the sample spectrum being taken after exposure of that wafer to the phosphonic acid.)

Turning to the fluorocarbon portion of the spectrum, we first examine the spectrum from an isotropic, polycrystalline sample of $F_8H_{11}PA$ dispersed in KBr (top spectrum of Figure 3). Many of the observed modes were assigned using results from previous studies.[38,42,43] Comparison with the F_8H_{11} bromide and F_8H_{11} alcohol (synthetic intermediates) allowed us to isolate vibrations resulting from the phosphonic acid. The asymmetric and symmetric P−O stretching vibrations appear at 1002 and 938 cm^{-1}, respectively.[52] We did not, however, observe the P═O stretch, as it is known to be broad when hydrogen bonded[52] and is likely obscured beneath C−F stretches in the region from 1150 to 1220 cm^{-1}. Also obscured by C−F stretches are known C−C stretching and C−C−C bending modes (with polarization parallel to the fluorocarbon helix) reported to be at 1220 cm^{-1}.[43]

When the bulk and IR−RAS 5 s immersion time spectra of Figure 3 are compared, several features regarding the structure of $F_8H_{11}PA$ SAMs on aluminum emerge. The primary feature is the modulation of mode intensities via the surface selection rule.[54] Modes polarized perpendicular to either the fluorocarbon helix (1146 cm^{-1}) or the hydrocarbon backbone (1471 cm^{-1}) are lower in intensity relative to modes polarized parallel to the fluorocarbon helix (1372, 1333, 706, and 658 cm^{-1}). Such a mode intensity modulation indicates that both the fluorocarbon helix and hydrocarbon chain of the molecule are oriented more toward the surface normal than parallel with the surface in the SAM. This near vertical orientation is in line with that expected given the ellipsometric thickness and contact angle data.

Further structural information is obtained from an examination of the modes arising from the phosphonic acid headgroup. First, the symmetric and asymmetric stretches of the P−O bonds of the phosphonic acid are not present in the IR−RAS spectra of the SAMs. Next, the broad feature at 1055−1072 cm^{-1} appears to be from the symmetric stretching mode of the PO_3^{2-} group, but we cannot rule out the possibility that it may be from a PO_3H^- vibration.[52] This evidence, combined with the observed loss of OH from the Al native oxide surface, is another indication that the phosphonic acids undergo a condensation reaction with surface bound Al−OH species, forming alumino-phosphonates. Finally, in IR−RAS spectra of $F_8H_{11}PA$, $H_{22}PA$, and $H_{16}PA$ SAMs there is a very broad region (700−950 cm^{-1}) where the baseline reproducibly dips below zero, suggesting the loss of Al−O bonds. As a result, some amount of etching of the native oxide is occurring in addition to the condensation reaction previously described.

When the spectra from longer immersion times in Figure 3 are compared to that from the 5 s dip time, we see continued change in vibrational band intensity. The modes showing

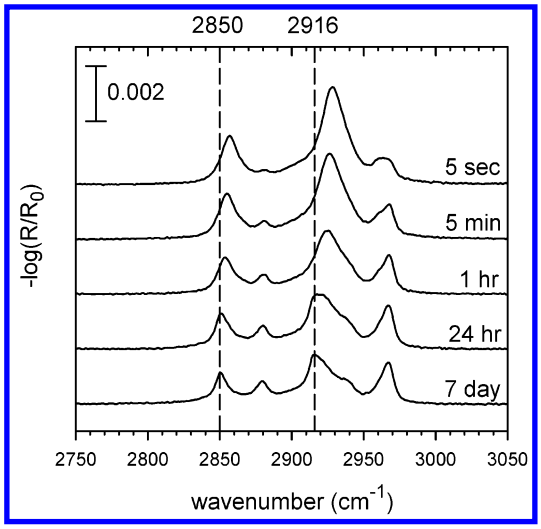

Figure 5. IR−RAS spectra of the C−H stretching region of $H_{16}PA$ SAMs on aluminum as a function of immersion time.

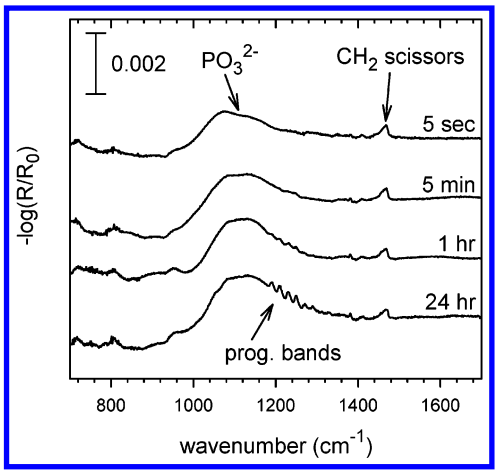

Figure 6. Low-frequency IR−RAS spectra of $H_{16}PA$ SAMs on aluminum as a function of immersion time.

intensity increases (662, 706, 1334, and 1372 cm^{-1}) are oriented parallel to the helical axis of the fluorocarbon segment (Table 3), while those decreasing in intensity (1155−1151 cm^{-1}) are oriented perpendicular to the helical axes. As immersion time in the coating solution increases, the fluorocarbon segment of the molecule orients itself such that its helical axis is more normal to the surface. Therefore, the modes at 1201 and 1250 cm^{-1} must be polarized perpendicular to the fluorocarbon helix since they decrease in intensity with increasing immersion time. Considering the IR−RAS data as a whole, the greatest intensity change occurred between the 5 s and 5 min immersion time samples. Small changes, however, continued through 24 h. Ellipsometric and contact angle data (Figure 1, Table 1) indicate no significant changes after 5 min immersion. Thus, it appears that the small changes after 5 min in solution are driven by subtle evolution in coverage and film structure to which ellipsometry and contact angle measurements are largely insensitive.

$H_{16}PA$. IR−RAS data on $H_{16}PA$ films are summarized in Figures 4−6 and Table 4. The high-frequency C−H stretching region of $H_{16}PA$ self-assembled films as a function of immersion time is shown in Figure 5. These IR spectra describe two types of changes as the film formation time increased. The first is seen in the shift of the two methylene stretching modes, d^+ and d^-, the former shifting from 2857 to 2850 cm^{-1}, the latter from 2929 to 2916 cm^{-1}, upon increasing film formation time

TABLE 4: Infrared Vibrational Modes for $H_{16}PA$ and $H_{22}PA$ Self-assembled Films on Aluminum Prepared through 7 day Dip Times with Abbreviations as in Table 3

mode description	transition dipole moment direction	mode frequency (cm^{-1}) $H_{16}PA$	$H_{22}PA$
$\nu_a(CH_3)$, r^-	ip CCC, along C−CH_3 bond	2967	2967
$\nu_s(CH_2)$, d^-	⊥, ⊥ to CCC plane	2916	2918
$\nu_s(CH_3)$ FR		2880	2880
$\nu_s(CH_2)$, d^+	⊥, in CCC plane	2850	2851
(CH_2) scissors	⊥ to chain	1467	1468
CH_3 def (sym), δ_{CH3}		1381	1382
CH_2 progression modes		1190−1270	1184−1305
$\nu_a(PO_3^{2-})/\nu(PO_2H^-)$		1131 br	1131 br
$\nu_s(PO_3^{2-})/\nu(PO_2H^-)$		∼1090 sh	
$r(CH_2)$	⊥ to chain	718	719

from 5 s to 7 days (see Figure 4). Such a shift has been previously associated with ordering of the methylene chain, as it becomes progressively more "all-trans".[55,56] The second change appears in the intensities of the d^+ and d^- peaks, which decreased with increasing immersion time. This is indicative of the alkyl chain orienting itself with its long axis more normal to the aluminum surface.[54]

In the low-frequency region of the $H_{16}PA$ monolayer spectra, we did not see dramatic changes over time, but subtle changes are still evident, and Figure 6 shows several important features. First, at about 1468 cm^{-1} is a scissoring mode of the $-CH_2-$ group. This mode is oriented perpendicular to the chain axis. It decreases slightly with time, indicating that the methylene chains orient themselves more normal to the surface as time progresses. Second, in the 1 h spectrum, we begin to see several small peaks between 1190 and 1290 cm^{-1}. These are often referred to as progression bands, resulting from an all-trans arrangement of the alkyl chain.[56] They are more distinct in the 24 h spectrum, again indicating that the chains are becoming more ordered. Finally, we note the broad features at 1130 and 1080 cm^{-1} that result from phosphonate binding to the Al surface. These are seen more clearly here than in spectra from the $F_8H_{11}PA$ SAMs in which they are obscured by C−F absorptions. For short immersion times the 1080 cm^{-1} peak is stronger with the 1130 cm^{-1} peak as a shoulder, but with time, the 1130 cm^{-1} peak becomes more intense. For SAMs on Al assembled from *n*-decanephosphonic acid, symmetric and asymmetric $R-PO_3^{2-}$ stretches (1055 and 1180 cm^{-1}) have been identified through PM−IR−RAS.[6] With this in mind, the spectral behavior we observe suggests that phosphonates initially bind to the Al surface in a tridentate fashion with the C−P bond essentially normal to the surface, maximizing the intensity of the symmetric PO_3^{2-} stretch at 1080 cm^{-1}. Phosphonates binding to the surface in the latter stages of self-assembly appear to have the C−P bond tilted from the surface normal, giving the asymmetric phosphonate stretch greater intensity. This behavior could also result from an increase in the extent of mono-[23] or bidentate[57] binding of the alkanephosphonic acid anion to the Al surface as self-assembly progresses.

$H_{22}PA$. Infrared spectra of $H_{22}PA$ self-assembled films on aluminum as a function of immersion time showed the same general trends as $H_{16}PA$ except to a much smaller extent (Figure 7). The frequencies of the d^+ and d^- modes changed only from 2852 and 2921 cm^{-1}, respectively, at 5 s immersion time to 2851 and 2918 cm^{-1} after 7 days, with no change occurring after 5 min (see Figure 4). In contrast, these frequencies in H_{16} films evolved steadily out to 7 days' immersion. However, Figure 7 shows clearly that the $H_{22}PA$ d^+ and d^- band intensities decreased steadily with immersion time, even out to 7 days, indicating H_{22} hydrocarbon chains were continuing to orient themselves more toward the surface normal.

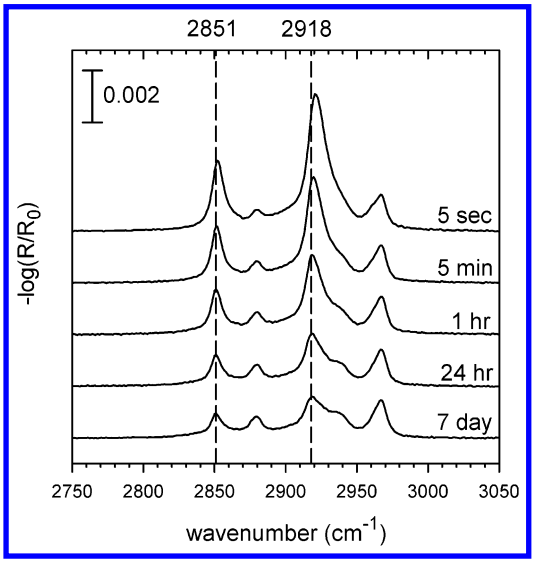

Figure 7. IR−RAS spectra of the C−H stretching region of $H_{22}PA$ SAMs on aluminum as a function of immersion time.

The low-frequency region of the infrared spectra of $H_{22}PA$ films on aluminum and its time dependence were essentially the same as seen for $H_{16}PA$. The only exception is that the progression bands appeared after only 5 s of dip time, becoming more distinct with time. Together with the C−H stretching region data, these results indicate that the hydrocarbon chains of $H_{22}PA$ order themselves conformationally more quickly than do those of $H_{16}PA$.

Examination of the C−H stretching region spectra of either $H_{16}PA$ or $H_{22}PA$ monolayers on aluminum revealed the evolution of the average tilt of the molecules. Initially, the d^+ and d^- methylene C−H stretching modes were quite high in intensity as seen in both Figures 5 and 7. With longer immersion time, these mode intensities decreased dramatically, even though coverage, as roughly estimated by ellipsometry, increased and then leveled off. This intensity decrease in two modes that are mutually perpendicular *and* perpendicular to the long axis of the alkyl chain can only be explained by a reorientation of the chain toward the surface normal. An estimate of the absolute orientation of the chains in $H_{16}PA$ and $H_{22}PA$ monolayers was deduced through a comparison with IR spectra of alkanethiol monolayers on copper, silver, and gold.[58] The ratio of intensities between methylene and methyl modes in the phosphonic acid films are much more like those obtained for thiols on copper or silver than on gold. To confirm that this was not merely a function of our infrared reflection accessory angle, we examined a sample of H_{18} thiol self-assembled on gold and obtained methylene/methyl mode intensity ratios in agreement with those reported previously.[58] This strongly suggests that the ultimate

tilt angle of the alkyl chains in the hydrocarbon PA monolayers is between 10 and 15° with respect to the surface normal. This is quite similar to the ~10° tilt of long-chain alkanoic acids on aluminum.[59] We expect the average chain tilt in $F_8H_{11}PA$ to also be low, by analogy with thiol monolayers in which fluorination reduces tilt angles slightly for F_8H_{11} and $F_{10}H_{11}$ thiols on gold relative to those of their hydrocarbon counterparts.[35] Consistent with our picture of low tilt angles for phosphonic acids on aluminum, Reven and co-workers[10] have presented evidence for vertical chain orientation in phosphonic acid monolayers on zirconia.

Messerschmidt and Schwartz[13] reported kinetic data for self-assembly of octadecanephosphonic acid ($H_{18}PA$) on sapphire at room temperature and 2 °C. Their results are difficult to compare directly with ours since their work was conducted with solutions of much lower concentration, but they observed trends in infrared spectra similar to those seen in our work with $H_{16}PA$ and $H_{22}PA$. At room temperature, the d^+ and d^- methylene bands shifted gradually to lower frequency with increasing immersion time, similar to our results for $H_{16}PA$. At 2 °C, the data behaved more like what we observed for $H_{22}PA$, in that the frequencies remained constant throughout film growth.

Mechanistic Aspects of Phosphonic Acid SAM Formation. Our experimental techniques of infrared spectroscopy, ellipsometry, and contact angle (all laterally averaging) cannot distinguish directly between two distinct modes of film growth: formation and growth of islands of ordered chains surrounded by disordered regions on one hand vs gradual ordering of a laterally homogeneous film on the other. The kinetic data from this study, however, suggest that formation of self-assembled monolayers from these alkane- and fluorinated alkanephosphonic acids occurs by distinctly different mechanisms. Infrared and ellipsometry data on $H_{16}PA$ and $H_{22}PA$ are consistent with initial formation of a disordered film that gradually orients upon further exposure to the coating solution. In related work, Messerschmidt and Schwartz[13] arrived at similar conclusions for formation of $H_{18}PA$ monolayers on sapphire at room temperature, while their data indicated ordered island formation at subambient temperatures. In our work, infrared spectra of $H_{16}PA$ and $H_{22}PA$ monolayers continued to evolve up to at least 7 days of exposure to the respective coating solutions, indicating a gradual trend toward ordered films. In contrast, the fluorinated system $F_8H_{11}PA$ reaches near-equilibrium film properties significantly faster than the hydrocarbon derivatives despite the lower $F_8H_{11}PA$ concentration employed. We propose that formation of this monolayer proceeds via deposition of islands of relatively ordered, already nearly vertically oriented molecules. By analogy with low-temperature deposition of $H_{18}PA$ on sapphire,[13] we cannot rule out the possibility that $H_{22}PA$ self-assembly on aluminum also proceeds via ordered islands. However, if it does, our IR intensity data demonstrate that the tilt angle of the chains in any such structures must decrease as film formation goes to completion.

A comprehensive picture emerges from the infrared spectra of the fluorinated and hydrocarbon systems. The hydrocarbon and fluorocarbon segments of $F_8H_{11}PA$ orient more toward the surface normal with increasing dip time, with most of the changes occurring in the first 5 min of immersion in the 1.2 mM solution. This is much like the behavior of $H_{16}PA$ and $H_{22}PA$, although differing markedly in the time scales involved. Self-assembly to an equilibrated monolayer film is much faster with the semifluorinated phosphonic acid than with the hydrocarbon derivatives; changes in the spectra of the latter were detected out to 24 h immersion and beyond, despite the higher concentrations (2.3−2.6 mM) utilized. Two possible reasons spring to mind for this difference. One is a solubility issue, in that $F_8H_{11}PA$ may be less soluble in ethanol and therefore would undergo self-assembly faster than the hydrocarbon analogues. This solubility difference could also manifest itself in micelle formation for $F_8H_{11}PA$ in ethanol, despite the observation that the surface tension of the solution[50] was very similar to that of pure (and already low surface tension) solvent. It may also be consistent with formation of relatively ordered islands (perhaps viewed as pseudo-admicelles?) even in the early stages of $F_8H_{11}PA$ self-assembly. Micelle formation has been documented in solutions of $C_8F_{17}CH_2CH_2SiCl_3$ in alkane solvents.[60] At this point we have no experimental evidence for formation of micelles in solutions of $F_8H_{11}PA$ in ethanol, but we hope to address this issue in future work. The second possibility is related to chain entanglement. The fluorocarbon groups of $F_8H_{11}PA$, being relatively rigid helices, may not be able to entangle as readily as the hydrocarbon PA chains; therefore, $F_8H_{11}PA$ self-assembly can reach its equilibrium state faster in the absence of steric encumbrance arising from chain entanglement. Also, if the initially disordered hydrocarbon PA films contain chains either lying flat or oriented with large tilt angles relative to the surface normal, this could produce lower rates of film formation and chain ordering through steric blocking of substrate binding sites.

We also propose that the difference in behavior between the phosphonic acids in this study can be couched in terms of the T_c concept originally advanced by Rondelez and co-workers[61] for alkyltrichlorosilane self-assembly. This model posits the existence of a critical temperature T_c for monolayer formation, below which optimum packing of the chains can be achieved. This behavior is related to the transition between liquid expanded and liquid compressed states in Langmuir monolayers. The value of T_c is a function of silane structure. For hydrocarbon silanes, T_c increases with increasing alkyl chain length. Hexadecyltrichlorosilane was found to have a value of T_c near room temperature, while docosyltrichlorosilane gave $T_c = 38$ °C.[61] If a similar relationship also holds for the alkanephosphonic acids, it would imply that room temperature, at which we have conducted all of our depositions, is near T_c for $H_{16}PA$ and well below T_c for $H_{22}PA$. This is consistent with the infrared data showing much faster chain ordering for the longer molecule. Rondelez and co-workers also correlated contact angle hysteresis with formation of monolayer films above or below T_c. Although we see no difference (Table 2) in hysteresis between $H_{16}PA$ and $H_{22}PA$ films at long immersion times, a significant difference is evident at short times (5−30 s). This picture can also account for the behavior of $F_8H_{11}PA$ provided that its T_c is significantly above room temperature. Rondelez and co-workers associated fluorinated silanes with low T_c, but the particular compounds considered in their work ($C_nF_{2n+1}CH_2CH_2SiCl_3$, $n = 8, 10$) have much shorter methylene spacers than $F_8H_{11}PA$. The effect of a chain such as F_8H_{11} on T_c in the Rondelez picture is unknown at present, but it seems reasonable that T_c could lie above room temperature and account for our observations that $F_8H_{11}PA$ behaves more like $H_{22}PA$ than it does $H_{16}PA$.

Viewed in the context of the infrared data, the difference in the time dependence of the ellipsometric film thicknesses for the fluorinated and hydrocarbon phosphonic acids (Figure 1) can be interpreted in at least two different ways. The slower increase in ellipsometric thickness for the hydrocarbon phosphonic acids may be consistent with the decrease in tilt angles of the chains as indicated by the IR band intensity data (Figures

5 and 7), as the time scales for the two phenomena are on the order of hours to days under the conditions studied here. On the other hand, the corresponding IR data for $F_8H_{11}PA$ indicate that the limiting orientational state is reached much faster, consistent with the ellipsometric film thickness which is essentially constant after 5 min immersion. An alternative interpretation of the ellipsometry data centers around a breakdown of the simple ellipsometric model used here. To extract film thicknesses, we assume that the film refractive index remains constant during the self-assembly process and is equal to the value expected for fully crystalline domains. The infrared data, with their indication of initially disordered $H_{16}PA$ and $H_{22}PA$ hydrocarbon chains, along with semifluorinated hydrocarbon chains in $F_8H_{11}PA$, which remain disordered during the entire self-assembly process, suggest that this assumption is not valid. The refractive index of incomplete hydrocarbon PA films is likely to be lower than our assumed value, which would lead to an underestimation of the film thickness. This is consistent with the data in Figure 1, which show that the hydrocarbon phosphonic acids approach equilibrium film thickness more slowly than does the fluorinated analogue. Thus, perhaps the ellipsometric data should not be taken as an absolute measure of coverage or chain density, but rather simply as another indication of the difference in behavior between the fluorinated and hydrocarbon phosphonic acids.

The failure of the methylene chain in $F_8H_{11}PA$ to achieve a fully ordered configuration as indicated by the d^+ and d^- frequencies is surprising in view of both the behavior of the hydrocarbon H_{16} and H_{22} phosphonic acids and the semifluorinated F_8H_{11} and $F_{10}H_{11}$ thiols.[37,42] All four of the latter systems display methylene mode frequencies which indicate fully ordered, crystalline chain configurations. One might be tempted to attribute the failure of $F_8H_{11}PA$ do to likewise to a methylene chain which is significantly shorter (11 carbons) than those in the hydrocarbon analogues (15 or 21 carbons). However, the fact that F_8H_{11} thiol does show ordered chains[42] suggests strongly that the different behavior of $F_8H_{11}PA$ is a headgroup effect. Perhaps the combination of the bulky fluorocarbon group and a bulky headgroup is enough to prevent complete ordering of the methylene segments, whereas for the thiol, with a smaller headgroup, this ordering can still occur.

To probe whether the disorder observed for the methylene chains in $F_8H_{11}PA$ was due to freezing in of metastable configurations during the room-temperature self-assembly, we conducted some experiments with annealing. IR−RAS spectra were recorded on an equilibrated monolayer sample at room temperature, then compared with those obtained after 3 min dwells at 150, 200, 250, and 300 °C in air. Essentially no change was observed in either the C−F or C−H regions of the spectra up to 250 °C. Beyond this temperature, the film appeared to undergo catastrophic degradation as evidenced by increases in methylene band frequencies, decreases in all monolayer band intensities, and a decrease in ellipsometric film thickness. Thus, heating showed no signs of inducing additional ordering in the methylene chains. This suggests that lack of mobility of the chains on the surface is not the issue, but that the disordered state of the methylene segments is indeed the equilibrium configuration. Further study of the thermal stability of these phosphonic acid monolayers is the subject of ongoing work in our laboratories.

Infrared spectroscopy provided by far the most sensitive tool for investigation of structural evolution in these self-assembled monolayers. The IR data indicated changes occurring in the films prepared at long immersion times which were not picked up by contact angle or ellipsometry measurements. Static and advancing water contact angles are particularly insensitive to many of the changes discussed here. Although water receding angles may show a slight increase at long exposure times for $F_8H_{11}PA$ and hence correlate with some of the subtle chain ordering effects indicated by the IR data, this was not the case for the hydrocarbon systems. Under the conditions utilized here, no significant changes in contact angles were noted after 1 h for $H_{16}PA$ and 5 min for $H_{22}PA$, even though the infrared spectra indicated that film ordering and chain orientation processes were far from complete by those times. Time scales on which the water contact angles evolved in these films seem to roughly correlate with those required for the methylene frequencies to reach their ultimate values—short for F_8H_{11} and H_{22} and longer for H_{16}.

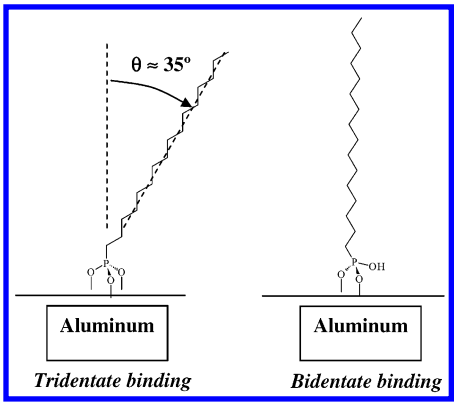

Figure 8. Schematic illustration of dependence of alkyl group tilt angle on phosphonate binding mode. The tilt angle for tridentate binding was estimated assuming a C−P bond normal to the substrate surface, C−C bond lengths of 1.54 Å, and C−C−C bond angles of 109.5°.

As noted earlier, the literature on phosphonic acid adsorption contains discussion of mono-,[23] di-,[57] and tridentate[29] binding of the phosphonate headgroup to metal oxide surfaces. However, our IR data alone do not allow us to determine a preferred binding mode in the systems studied here. We note that tridentate binding would give chains oriented at tilt angles of about 35° from the surface normal for the hydrocarbon phosphonic acids (Figure 8), while our IR data suggest considerably less tilt. Thus, perhaps these observations are more consistent with mono- or bidentate binding, with the unreacted acid OH functionality available for hydrogen bonding to adjacent molecules. Also, within this framework, the evolution noted above from tridentate to lower binding modes as film formation proceeds is consistent with the decrease in alkyl chain tilt angles indicated by the IR−RAS data.

Poor solubility of $H_{22}PA$ prevented use of ethanol as the common solvent for our studies. The question arises, therefore, as to whether solvent effects can be the origin of the disparate behaviors we observe. We do not believe this to be the case based on results from experiments with $H_{16}PA$ and $F_8H_{11}PA$ on films deposited from THF. These solutions were found in general to be less stable than those in ethanol, and were prone to development of precipitate, especially with $F_8H_{11}PA$, within days of preparation. This led to significant deposition of excess material on wafers treated for long immersion times. In the case of $F_8H_{11}PA$, removal of these excess deposits required sonication. Although ethanol solutions could also develop precipitate after weeks of storage at room temperature, when freshly prepared they remained clear and precipitate-free during the 7-day duration of our experiments. The nature and origin of these precipitates is unknown at present but is under investigation. These considerations notwithstanding, IR, ellipsometric,

and contact angle data on films from $H_{16}PA$ and $F_8H_{11}PA$ were quite similar to those for analogous films delivered from ethanol. In view of these results, we consider solvent effects, at least with respect to ethanol vs THF, of little consequence.

Comparison with Other SAM Systems. Finally, it is instructive to compare the results of our kinetic study with literature results on other SAM systems. An acceleration in the rate of self-assembly for perfluoroalkyl- vs alkyl-substituted amphiphiles has been noted previously for trichlorosilanes.[51] Immersion times of 1−3 min for formation of optimum monolayer films of a fluorinated trichlorosilane[47] under conditions (concentration, film formation temperature) similar to those used here are consistent with our kinetic observations for $F_8H_{11}PA$. We are not aware of kinetic studies comparing rates of SAM formation for alkanethiols and fluorinated alkanethiols. Our kinetic data for the hydrocarbon phosphonic acids on aluminum show similarities when compared with data on the analogous thiols self-assembling on gold.[45] In this work, wafer samples emerged autophobic after just a few seconds' immersion in 1 mM solutions of alkanethiol, and ellipsometric thicknesses rose rapidly within the first few minutes, followed by a period of some hours during which the equilibrium values were reached.

The kinetics of alkanethiol self-assembly on gold have been extensively studied,[2b,c] with a number of reports in this area utilizing infrared spectroscopy.[62−64] In cases where the amphiphile concentration was in the same regime as in our work (1−3 mM), the results were quite similar to ours, with the caveat that alkanethiols self-assemble faster on gold than do alkanephosphonic acids on aluminum native oxide.[63,64] Shon and Lee described the self-assembly kinetics of heptadecanethiol on gold, noting that a limiting value for the d^- peak of 2919 cm^{-1} was reached after only 1 h.[63] As with our results, they reported a decrease in intensity of the d^+ and d^- modes with increasing time, despite the fact that coverage (as measured by ellipsometry) increased. Pan and co-workers reported similar phenomena in the self-assembly of 16-mercapto-1-hexadecanol on gold: from a 1 mM solution, they observed a decrease in the peak position of d^- and its intensity over time.[64] Their interpretation was the same as ours. As coverage increases, the chains attain a more ordered, all-trans conformation and the chains orient themselves closer to the surface normal.

Our results also line up well with other studies on hydrocarbon phosphonic acids. As pointed out earlier, infrared spectra for $H_{16}PA$ and $H_{22}PA$ on aluminum share several common features with the IR data of Messerschmidt and Schwartz[13] for self-assembly of $H_{18}PA$ on sapphire at ambient and subambient temperatures. At low temperature, $H_{18}PA$ on sapphire seems to behave more like $H_{22}PA$ on aluminum at room temperature, whereas at room-temperature $H_{18}PA$ on sapphire and $H_{16}PA$ on aluminum behave similarly. The temperature dependence of $H_{18}PA$ self-assembly on sapphire was also discussed by Messerschmidt and Schwartz[13] in terms of the Rondelez et al.[61] T_c formalism. Below T_c, film formation proceeds via deposition of ordered islands, whereas above T_c self-assembly involves initial formation of a disordered monolayer which gradually orients and orders as coverage increases.

Bram, Jung, and Stratmann[21] have reported a study, by XPS, AES, and IR, of self-assembly of an unspecified alkanephosphonic acid on aluminum from an unspecified solvent. While detailed comparisons are difficult, their infrared data are consistent with ours, as they reported methylene frequencies at ∼2850 and 2920 cm^{-1} at long exposure times and slightly higher values at short times. They also concluded that while the bulk of the film assembly appeared to be complete within a few minutes, chain organizational processes continued over a span of several days, in qualitative agreement with the results of our study.

Lewington et al. performed a study in which they used contact angle to monitor the formation of ethane-, propane-, butane-, and decanephosphonic acid SAMs on aluminum.[6] For decanephosphonic acid ($H_{10}PA$) self-assembled on hydrated aluminum from 5 mM solution in ethanol, they reported a static water contact angle of 94° after 10 days immersion time. For one sample immersed for 5 days they reported FTIR data: CH_2 d^+ and d^- peak positions of 2853 and 2924 cm^{-1}. For a SAM made from 24 h immersion in 0.1% dodecanephosphonic acid (3.2 mM $H_{12}PA$) in ethanol, we recorded not only a significantly higher static contact angle of 110°, but also higher d^+ and d^- peak positions of 2855 and 2926 cm^{-1}. It is possible that our higher contact angle values are due to our aluminum surface deposited by thermal evaporation being rougher than their aluminum deposited through magnetron sputtering. Our infrared peak positions (2852 and 2923 cm^{-1}, for d^+ and d^-, respectively) drop to approximately the same values reported by Lewington et al. if the immersion time is extended for several weeks. Our FTIR data after 24 h and several weeks' immersion bracket their 5-day data when no pretreatment of the aluminum surface is performed.

Our observations of infrared spectra indicative of ordered films for equilibrated self-assembled monolayers of $H_{16}PA$ and $H_{22}PA$ on aluminum are consistent with previous literature data. Octadecanephosphonic acid has been extensively studied on a range of substrates, and in general gives films showing infrared spectra consistent with ordered chains (methylene frequencies 2846−2852, 2914−2921 cm^{-1}) on aluminum,[18] titania,[15,23] copper,[17] mica,[20] and zirconia.[23] For alumina, however, Reven and co-workers[23] reported the formation of a bulk aluminophosphonate phase upon treatment with $H_{18}PA$. Our ellipsometric results show no evidence for deposition of such phases on aluminum native oxide for the phosphonic acids and experimental conditions studied here.

We know of no literature describing detailed study of semifluorinated alkanephosphonic acids with which to compare our results. Such species are known, primarily through disclosures in the patent literature.[65] However, as far as we are aware our study is the first to probe the details of self-assembly for this class of materials. Fluorinated monophosphate ester self-assembly has received some scrutiny in recent literature,[66] although structurally these materials are quite different from $F_8H_{11}PA$ studied here, and direct comparisons are difficult.

Conclusions

We have used infrared spectroscopy, ellipsometry, and contact angles to monitor kinetics of self-assembled film formation by three alkanephosphonic acids—**1** ($F_8H_{11}PA$), **2** ($H_{16}PA$), and **3** ($H_{22}PA$)—on aluminum native oxide from dilute solution in organic solvents at room temperature. The most significant observation from our study is the lack of ordering in the methylene segment of the semifluorinated $F_8H_{11}PA$ self-assembled films, even at long assembly times. This contrasts with the ordered chains in equilibrium films from $H_{16}PA$ and $H_{22}PA$ (which bracket $F_8H_{11}PA$ in terms of the length of their alkyl chains), as well as the ordered methylene segments in SAMs prepared from F_8H_{11} and $F_{10}H_{11}$ thiols on gold.[37,42] We attribute this behavior to steric effects of the fluorocarbon segment and the phosphonic acid headgroup. Thus, $F_8H_{11}PA$ represents an amphiphile system in which bulky head and tail

groups prevent an interposed hydrocarbon segment from ordering.[48a] For all three phosphonic acids, negative peaks attributed to loss of Al−OH groups in the infrared spectra of the monolayers are consistent with a condensation reaction between the acids and surface hydroxyls to form bound aluminophosphonate salts.

With respect to film formation kinetics, all of our data indicate that $F_8H_{11}PA$ approaches its equilibrium film structure considerably faster than the hydrocarbon phosphonic acids. For $F_8H_{11}PA$, ellipsometric film thicknesses, water static, and advancing contact angles, hexadecane contact angles, and methylene band infrared frequencies and intensities all reach their equilibrium values within 5−10 min exposure of the aluminum substrate to a 0.1 wt % solution of phosphonic acid. C−F band intensities and water receding angles continue to change slightly as film assembly times increase, indicating the occurrence of subtle organizational processes involving the fluorocarbon segment. For the hydrocarbon species H_{16} and $H_{22}PA$, the behavior is quite different. Methylene band infrared frequencies for films from both materials on aluminum decrease to values indicative of ordered chains, within 5 min for $H_{22}PA$ but over days for $H_{16}PA$; however, band intensities decrease over the span of several days for both species. Water contact angles for the hydrocarbon PA films change in the same manner as the methylene band infrared frequencies—quickly for H_{22}, more gradually for H_{16}—while the ellipsometric thicknesses for both H_{16} and H_{22} require hours to reach their equilibrium values.

We interpret the dependence of film formation kinetics on structure in terms of the T_c formalism proposed by Rondelez and co-workers.[61] Within this framework, $F_8H_{11}PA$ and $H_{22}PA$ at room temperature are probably below their values of T_c, leading to more rapid film assembly, whereas $H_{16}PA$ at room temperature is probably above its T_c, leading to slower film growth. Additionally, we suggest that the faster film formation kinetics exhibited by $F_8H_{11}PA$ relative to the hydrocarbons may be due to chain entanglement and solubility effects, and that the semifluorinated species may self-assemble as islands of approximately vertically oriented chains that fill in as the film approaches full coverage. $H_{22}PA$ may also deposit as islands, but in contrast, film formation for $H_{16}PA$ probably involves initially disordered chains with higher tilt angles that order and reorient as film assembly proceeds.

Acknowledgment. The authors are grateful to Drs. V. W. Jones and D. A. Weil (3M Corporate Analytical Technology Center) for collection of AFM and high-resolution mass spectrometry data, respectively.

Supporting Information Available: Text giving experimental details for the preparations of the three phosphonic acids utilized in this study: **1** ($F_8H_{11}PA$), **2** ($H_{16}PA$), and **3** ($H_{22}PA$). This material is available free of charge via the Internet at http://pubs.acs.org.

References and Notes

(1) Ulman, A. *An Introduction to Ultrathin Organic Films*; Academic Press: San Diego, CA 1991.

(2) For some recent reviews, see for instance: (a) Everhart, D. S. in *Handbook of Applied Surface and Colloid Chemistry*; Holmberg, K., Ed.; John Wiley and Sons: West Sussex, England, 2002; Volume 2, Chapter 6. (b) Schwartz, D. K. *Annu. Rev. Phys. Chem.* **2001**, *15*, 107−137. (c) Schreiber, F. *Prog. Surf. Sci.* **2000**, *65*, 151−256. (d) Ulman, A. *Chem. Rev.* **1996**, *96*, 1533−1554. (e) Delamarche, E.; Michel, B.; Biebuyck, H. A.; Gerber, C. *Adv. Mater.* **1996**, *8*, 719−729. (f) Xu, J.; Li, H. L. *J. Colloid Interface Sci.* **1995**, *176*, 138−149.

(3) See, for instance: (a) U.S. Patent 5,266,222, 1993. (b) U.S. Patent 5,284,707, 1994.

(4) (a) U.S. Patent 6,433,359, 2002. (b) Beebe, J. M.; Engelkes, V. B.; Miller, L. L.; Frisbie, C. D. *J. Am. Chem. Soc.* **2002**, *124*, 11268−11269. (c) Selzer, Y.; Cahen, D. *Adv. Mater.* **2001**, *13*, 508−511. (d) Cui, J.; Huang, Q.; Wang, Q.; Marks, T. J. *Langmuir* **2001**, *17*, 2051−2054. (e) Appleyard, S. F. J.; Willis, M. R. *Opt. Mater.* **1998**, *9*, 120−124.

(5) Sinapi, F.; Forget, L.; Delhalle, J.; Mekhalif, Z. *Surf. Interface Anal.* **2002**, *34*, 148−154.

(6) Lewington, T. A.; Alexander, M. R.; Thompson, G. E.; McAlpine, E. *Surf. Eng.* **2002**, *18*, 228−232.

(7) Bakiamoh, S. B.; Blanchard, G. J. *Langmuir* **2002**, *18*, 6246−6253.

(8) Brewer, S. H.; Brown, D. A.; Franzen, S. *Langmuir* **2002**, *18*, 6857−6865.

(9) Pawsey, S.; Yach, K.; Reven, L. *Langmuir* **2002**, *18*, 5205−5212.

(10) Yim, C. T.; Pawsey, S.; Morin, F. G.; Reven, L. *J. Phys. Chem. B* **2002**, *106*, 1728−1733.

(11) Breen, T. L.; Fryer, P. M.; Nunes, R. W.; Rothwell, M. E. *Langmuir* **2002**, *18*, 194−197.

(12) Doudevski, I.; Schwartz, D. K. *J. Am. Chem. Soc.* **2001**, *123*, 6867−6872.

(13) Messerschmidt, C.; Schwartz, D. K. *Langmuir* **2001**, *17*, 462−467.

(14) Sahoo, Y.; Pizem, H.; Fried, T.; Golodnitsky, D.; Burstein, L.; Sukenik, C. N.; Markovich, G. *Langmuir* **2001**, *17*, 7907−7911.

(15) Gawalt, E. S.; Avaltroni, M. J.; Koch, N.; Schwartz, J. *Langmuir* **2001**, *17*, 5736−5738.

(16) Kanan, S. M.; Tripp, C. P. *Langmuir* **2001**, *17*, 2213−2218.

(17) Baker, M. V.; Jennings, G. K.; Laibinis, P. E. *Langmuir* **2000**, *16*, 3288−3293.

(18) Van Alsten, J. G. *Langmuir* **1999**, *15*, 7605−7614.

(19) Goetting, L. B.; Deng, T.; Whitesides, G. M. *Langmuir* **1999**, *15*, 1182−1191.

(20) Woodward, J. T.; Doudevski, I.; Sikes, H. D.; Schwartz, D. K. *J. Phys. Chem. B* **1997**, *101*, 7535−7541.

(21) Bram. C.; Jung, C.; Stratmann, M. *Fresenius J. Anal. Chem.* **1997**, *358*, 108−111.

(22) Gao, W.; Dickinson, L.; Grozinger, C.; Morin, F. G.; Reven, L. *Langmuir* **1997**, *13*, 115−118.

(23) Gao, W.; Dickinson, L.; Grozinger, C.; Morin, F. G.; Reven, L. *Langmuir* **1996**, *12*, 6429−6435.

(24) Woodward, J. T.; Schwartz, D. K. *J. Am. Chem. Soc.* **1996**, *118*, 7861−7862.

(25) Woodward, J. T.; Ulman, A.; Schwartz, D. K. *Langmuir* **1996**, *12*, 2, 3626−3629.

(26) Gardner, T. J.; Frisbie, C. D.; Wrighton, M. S. *J. Am. Chem. Soc.* **1995**, *117*, 6927−6933.

(27) Folkers, J. P.; Gorman, C. B.; Laibinis, P. E.; Buchholz, S.; Whitesides, G. M. *Langmuir* **1995**, *11*, 813−824.

(28) Randon, J.; Blanc, P.; Paterson, R. *J. Membr. Sci.* **1995**, *98*, 119−129.

(29) (a) Ramsier, R. D.; Henriksen, P. N.; Gent, A. N. *Surf. Sci.* **1988**, *203*, 72−88. (b) Davies, P. R.; Newton, N. G. *Appl. Surf. Sci.* **2001**, *181*, 296−306.

(30) Castner, D. G.; Grainger, D. W., Eds. *Fluorinated Surfaces, Coatings, and Films*; ACS Symposium Series 787; American Chemical Society: Washington, DC, 2001.

(31) Colorado, R., Jr.; Lee, T. R. *Langmuir* **2003**, *19*, 3288−3296.

(32) Mekhalif, Z.; Massi, L.; Guittard, F.; Geribaldi, S.; Delhalle, J. *Thin Solid Films* **2002**, *405*, 186−193.

(33) Wagner, A. J.; Carlo, S. R.; Vecitis, C.; Fairbrother, D. H. *Langmuir* **2002**, *18*, 1542−1549.

(34) Cheadle, E. M.; Batchelder, D. N.; Evans, S. D.; Zhang, H. L.; Fukushima, H.; Miyashita, S.; Graupe, M.; Puck, A.; Shmakova, O. E.; Colorado, R., Jr.; Lee, T. R. *Langmuir* **2001**, *17*, 6616−6621.

(35) Naud, C.; Calas, P.; Commeyras, A. *Langmuir* **2001**, *17*, 4851−4857.

(36) Tamada, K.; Ishida, T.; Knoll, W.; Fukushima, H.; Colorado, R., Jr.; Graupe, M.; Shmakova, O. E.; Lee, T. R. *Langmuir* **2001**, *17*, 1913−1921.

(37) Fukushima, H.; Seki, S.; Nishikawa, T.; Takiguchi, H.; Tamada, K.; Abe, K.; Colorado, R., Jr.; Graupe, M.; Shmakova, O. E.; Lee, T. R. *J. Phys. Chem. B* **2000**, *104*, 7417−7423.

(38) Frey, S.; Heister, K.; Zharnikov, M.; Grunze, M.; Tamada, K.; Colorado, R., Jr.; Graupe, M.; Shmakova, O. E.; Lee, T. R. *Isr. J. Chem.* **2000**, *40*, 81−97.

(39) Graupe, M.; Takenaga, M.; Koini, T.; Colorado, R., Jr.; Lee, T. R. *J. Am. Chem. Soc.* **1999**, *121*, 3222−3223.

(40) Miura, Y. F.; Takenaga, M.; Koini, T.; Graupe, M.; Garg, N.; Graham, R. L. Jr.; Lee, T. R. *Langmuir* **1998**, *14*, 5821−5825.

(41) Kim, H. I.; Koini, T.; Lee, T. R.; Perry, S. S. *Langmuir* **1997**, *13*, 7192−7196.

(42) Tsao, M. W.; Hoffmann, C. L.; Rabolt, J. F.; Johnson, H. E.; Castner, D. G.; Erdelen, C.; Ringsdorf, H. *Langmuir* **1997**, *13*, 4317−4322.

(43) Lenk, T. J.; Hallmark, V. M.; Hoffmann, C. L. Rabolt, J. F.; Castner, D. G.; Erdelen, C.; Ringsdorf, H. *Langmuir* **1994**, *10*, 4610−4617.

(44) Laibinis, P. E.; Whitesides, G. M. *J. Am. Chem. Soc.* **1992**, *114*, 1990−1995.

(45) Bain, C. D.; Troughton, E. B.; Tao, Y.-T.; Evall, J.; Whitesides, G. M.; Nuzzo, R. G. *J. Am. Chem. Soc.* **1989**, *111*, 321−335.

(46) Genzer, J.; Efimenko, K.; Fischer, D. A. *Langmuir* **2002**, *18*, 9307−9311.

(47) Pellerite, M. J.; Wood, E. J.; Jones, V. W. *J. Phys. Chem. B* **2002**, *106*, 4746−4754. This reference also cites a list of leading references describing work on fluorinated silane monolayers.

(48) There are a number of reports on studies of Langmuir films of partially fluorinated alkanecarboxylic acids. See for example: (a) Ren, Y.; Iimura, K.; Kato, T. *J. Phys. Chem. B* **2002**, *106*, 1327−1333. (b) Lehmler, H.-J.; Bummer, P. *J. Fluorine Chem.* **2002**, *117*, 17−22. (c) Gaines, G. L., Jr., Chapter 1 in *Characterization of Organic Thin Films*; Ulman, A., Ed.; Butterworth-Heinemann: Stoneham, MA, 1995.

(49) Parikh, A.; Allara, D.; Azouz, I. B.; Rondelez, F. *J. Phys. Chem.* **1994**, *98*, 7577−7590.

(50) Surface tension measurements were made at room temperature on different batches of solution on different days, using DuNouy ring (Kruss K10ST digital tensiometer) and Wilhelmy (Kruss K100 Processor Tensiometer with platinum plate) methods. For the ring measurements, results were as follows: ethanol, 21.8 dyn/cm; 0.1 wt % F_8H_{11}PA in ethanol, 22.2 dyn/cm. For the Wilhelmy plate measurements, results were as follows: ethanol, 22.26 dyn/cm; 0.1 wt % F_8H_{11}PA in ethanol, 22.22 dyn/cm, with standard deviations on both values of 0.05 dyn/cm. The literature value for surface tension of ethanol is 22.39 ± 0.1 dyn/cm at 20 °C (Jasper, J. J. *J. Phys. Chem. Ref. Data* **1972**, *1*, 841−1009).

(51) Banga, R.; Yarwood, J.; Morgan, A. M.; Evans, B.; Kells, J. *Langmuir* **1995**, *11*, 4393−4399.

(52) Thomas, L. C. *Interpretation of the Infrared Spectra of Organophosphorus Compounds*; Heyden: London, 1974.

(53) Knoezinger, H.; Ratnasamy, P. *Catal. Rev.—Sci. Eng.* **1978**, *17*, 31−69.

(54) For vibrational modes on a metal surface probed by infrared radiation, there is a surface selection rule that allows only the component of a vibration's transition dipole moment perpendicular to the metal surface to be observed. See: Greenler, R. G. *J. Chem. Phys.* **1966**, *44*, 310−315. Consequently, for C−H stretches that have their transition dipole moments normal to the long axis of the H_{16}PA chain a decrease in intensity means that the C−H bonds are orienting themselves more parallel with the metal surface, and thus the long axis of the chain is more normal to the metal surface.

(55) Snyder, R. G.; Strauss, H. L.; Elliger, C. A. *J. Phys. Chem.* **1982**, *86*, 5145−5150.

(56) Porter, M. D.; Bright, T. B.; Allara, D. L.; Chidsey, C. E. D. *J. Am. Chem. Soc.* **1987**, *109*, 3559−3568.

(57) A mixture of mono- and bidentate bonding has been proposed for octadecyl monophosphate on tantalum oxide: Textor, M.; Ruiz, L.; Hofer, R.; Rossi, A.; Feldman, K.; Hähner, G.; Spencer, N. C. *Langmuir* **2000**, *16*, 3257−3271.

(58) Laibinis, P. E.; Whitesides, G. M.; Allara, D. L.; Tao, Y.-T.; Parikh, A. N.; Nuzzo, R. G. *J. Am. Chem. Soc.* **1991**, *113*, 7152−7167.

(59) Allara, D. L.; Nuzzo, R. G. *Langmuir* **1985**, *1*, 52−66.

(60) Bunker, B. C.; Carpick, R. W.; Assink, R. A.; Thomas, M. L.; Hankins, M. G.; Voigt, J. A.; Sipola, D.; de Boer, M. P.; Gulley, G. L. *Langmuir* **2000**, *16*, 7742−7751.

(61) Brzoska, J. B.; Ben Azouz, I.; Rondelez, F. *Langmuir* **1994**, *10*, 4367−4373.

(62) Bensebaa, F.; Voicu, R.; Huron, L.; Ellis, T. H.; Kruus, E. *Langmuir* **1997**, *13*, 5335−5340.

(63) Shon, Y. S.; Lee, T. R. *J. Phys. Chem. B* **2000**, *104*, 8182−8191.

(64) Pan, S.; Belu, A. M.; Ratner, B. D. *Mater. Sci. Eng. C* **1999**, *7*, 51−58.

(65) See for instance: (a) U.S. Patent 6,380,101, 2002. (b) European Patent Application EP 606,640, 1994.

(66) McNatt, J. S.; Morgan, J. M.; Farkas, N.; Ramsier, R. D.; Young, T. L.; Rapp-Cross, J.; Espe, M. P.; Robinson, T. R.; Nelson, L. Y. *Langmuir* **2003**, *19*, 1148−1153.